PAPER

Check for updates

Novel SLIPS based on the photo-thermal MOFs with enhanced anti-icing/de-icing properties†

Xinzuo Fang, [iD] * Yufan Liu, Sheng Lei, Chuangquan Li, Junfei Ou [iD] and Alidad Amirfazli [iD]

A photo-thermal anti-icing/de-icing SLIPS coating is designed based on porous light-responsive MOFs. Due to the strong light absorption and high light-thermal conversion, the as-synthetic SCMOFs exhibited prolonged freezing delay time and depressed water crystallization point under light irradiation. Meantime, the SCMOFs exhibit good deicing properties. With the irradiation, the half-melted ice slips off quickly.

Introduction

Ice formation and accretion on the surfaces of outdoor infrastructures is a critical issue in daily life. The ice adhering to aircraft vehicles, wind turbines and power transmission lines often causes severe safety problems and enormous energy losses.[1–5] In order to solve the ice formation and accretion, many methods and technologies have attracted wide attention.[6–8]

Currently, the conventional strategies for anti-icing/de-icing can be categorized into active anti-icing/de-icing methods and passive anti-icing methods.[9–11] The active methods need an external energy input to overcome the problem. Many active de-icing approaches have been developed, including mechanical breakage, cutting, thermal, or electro-impulse methods. Among these active approaches, the widely used active anti-icing/de-icing method is based on the electro-thermal techniques. The heat is generated by the electro-thermal materials or components and then used to melt the ice with high efficiency.[12–14] At the same time, the passive anti-icing methods without external energy input have also attracted much attention due to the convenient preparation and lower surface ice adhesion.[15–18] The super-hydrophobic surfaces (SHS) can prevent ice formation and reduce the ice adhesion due to the super-high water contact angles (≥150°) for effective water repellency, which is considered as a viable method for application.[19,20] Meantime, inspired by the Nepenthes pitcher plant, slippery lubricant-infused porous surface (SLIPS) have attracted much attention as a passive anti-icing methods.[21–23]

Even though both active and passive anti-icing/de-icing methods have exhibited good performance, there are some limits existed. The active methods are often expensive and also

School of Materials Engineering, Jiangsu University of Technology, Changzhou, 213001, P. R. China. E-mail: 2017500077@jsut.edu.cn

† Electronic supplementary information (ESI) available. See https://doi.org/10.1039/d2ra02046g

involve more energy consumption in the electro-thermal method. Melted ice can refreeze at a different location on the surface, thus only transferring the problem to another part of the surface. The passive methods involve fewer of these types of problems and do not require an external energy input, but exhibit low efficiency for the de-icing. Hence, it is essential to find a more energy-saving and efficient method for the control of ice formation and accretion. Developing a new method integrated the advantages of active and passive anti-icing/de-icing methods will be a promising work.

Metal–organic frameworks (MOFs) are crystalline materials with high Brunauer–Emmett–Teller (BET) surface areas and ordered porous structure. Constructed by the versatile organic ligands and metal ions, the MOFs have been widely investigated in many field.[24–27] Recently, due to the abundant porous structure for the storage of lubricant, the MOFs have been used as a good candidate to build stable SLIPS. At the same time, thanks to the variety and modifiability of MOFs, some MOFs possess the property like semiconductor, exhibiting the electro-thermal or photo-thermal phenomenon. Thus, the photo-thermal MOFs can be chosen for the active de-icing methods. Taking advantage of the MOFs used as substrate, the MOFs can link the active and passive anti-icing methods as an intermediary to overcome the energy waste and weak efficiency.

Inspired by this, a photo-thermal MOFs are chosen as the porous structure to build the SLIPS. Containing the 2,3,6,7,10,11-hexahydroxytriphenylene ($H_{12}C_{18}O_6$, HHTP) and Cu in the frameworks, the Cu-CAT-1 MOFs exhibit excellent light absorption and photo-thermal ability.[26,27] Meantime, the extended honeycomb structure with hexagonal pores serves as a reservoir to store and replenish the lubricant. As above, the Cu foil was chosen as the substrate, and $Cu(OH)_2$ nanowires (NWs) were first obtained and then used as a sacrificial template to synthesize Cu-CAT-1 MOFs. Finally, the poly(methyhydrosiloxane) as a lubricant was infused into the surface structure to obtain the SLIPS based on the Cu-CAT-1 MOFs

(denoted as SCMOFs). Owing to the porous structure and good light-thermal conversion, the SCMOFs exhibits good anti-icing/de-icing behaviors, efficiently lowing the ice nucleation temperature and delaying the freezing point of water.

Experimental

Materials and methods

Copper foil (purity > 99%) was purchased from Anping Tairun Wire Mesh Co., Ltd. Sodium hydroxide, ammonium persulfate and 2,3,6,7,10,11-hexahydroxytriphenylene (HHTP, 95%) were purchased from Shanghai Chemical Reagent Co., Ltd. Poly(-methyhydrosiloxane) with different viscosity were obtained from Macklin Inc. All chemicals were used without any further purification.

Characterizations

Powder X-ray diffraction (XRD) patterns were carried out at the Japan Rigaku DMax-γA rotation anode X-ray diffractometer. Scanning electron microscopy (SEM) images were obtained from the field emission scanning electron microanalyzer (Sigma 500, scanning electron microscope). Infrared (IR) images and surface temperatures were recorded on a Fluke Ti450 Infrared Camera (Fluke, USA). The surface roughness was characterized by confocal laser scanning microscopy (CLSM, KEYENCE VK-X). The surface wettability of the samples were performed through a Kruss DSA30 contact angle analyzer.

Anti-icing experiments

The anti-icing performance of samples can be estimated by measuring the freezing delay time of water droplets and water crystallization point with and without the light irradiation.

The tests of freezing delay time were performed on the Kruss DSA30 assisted with a cooling stage under N_2 atmosphere. A water droplet was dripped onto the surface of samples and the samples fixed on the cooling stage at the temperature of −15 °C. The time was recorded as the droplet began to freeze with change from transparency to non-transparency due to the different reflectivity between water and ice.

The water crystallization point were also performed on the Kruss DSA30 assisted with a cooling stage under N_2 atmosphere. A water droplet was dripped onto the surface of samples and the samples fixed on the cooling stage with the temperature cooled at the speed of 5 °C min^{-1} from 25 °C to −20 °C. The point was observed and recorded by microscope when the transparency changed.

The light-thermal deicing properties of samples were tested using the same method with a sunlamp light (150 W) as a solar simulator source.

Preparation of the SCM

Synthesis of Cu(OH)₂ NWs. Desired size of commercial Cu foil (1.5 cm × 1.5 cm) was washed with dilute H_2SO_4 (5 vol%), and Milli-Q water to remove the surface oxide. The synthesis of Cu(OH)₂ NWs was realized *via* two room-temperature reactions including an alkali assisted oxidation process and a modification process. Briefly, the washed Cu foil was soaked in 25 mL mixture solution containing 12.5 mL of 5 M NaOH, 2.5 mL of 1 M $(NH_4)_2S_2O_8$, and 10 mL of H_2O for 45 min at room temperature to form Cu(OH)₂ microstructure on the surface.

Synthesis of Cu-CAT-1 MOFs. To grow Cu-CAT-1 MOF crystals on Cu(OH)₂ NWs, the Cu(OH)₂ NWs on Cu foil were immersed into a mixture solution of Milli-Q water and DMF (v/v = 10 : 1) containing 30 mg of HHTP in a Petri dish, and then put into a pre-heated oven at 70 °C for 20 min. After naturally cooled down to room temperature, the resulted sample was thoroughly rinsed with acetone, and the Cu-CAT-1 MOFs was obtained.

Synthesis of SLIPS based on Cu-CAT-1 MOFs (SCMOFs). The poly(methyhydrosiloxane) was chosen as the lubricant. The Cu-CAT-1 MOFs grown on the foil were erected on the vessel containing the poly(methyhydrosiloxane). After thoroughly infusion and capillary action, the SCMOFs was obtained.

For comparison, the SLIPS based on the Cu(OH)₂ NWs were also prepared with similar method. The as-synthetic sample was denoted as SCNWs.

Results and discussion

The light-responsive anti-icing/de-icing SCMOFs sample was obtained based on the mixed structure of Cu-CAT-1 MOFs and Cu(OH)₂ NWs. The Cu(OH)₂ NWs was first grown on the Cu foil and then the Cu-CAT-1 was prepared using the Cu(OH)₂ NWs as template and Cu source. As shown in Fig. 1a, the X-ray diffraction (XRD) was applied to confirm, peaks at 4.8°, 9.5° and 12.6° indicate the successful synthesis of Cu-CAT-1, which can be matched with the ref. 27. Other peaks for Cu(OH)₂ and for Cu can also be observed, indicating that Cu(OH)₂ NW backbones and Cu foil still exist after the reaction. The surface morphology was also observed by the SEM. The Cu(OH)₂ NWs was grown with similar diameter and length on Cu foil, after reacted with the HHTP, the Cu-CAT-1 was grown around the Cu(OH)₂ NWs with the surface rougher, as exhibited from the SEM images. At the same time, the confocal laser scanning microscopy was taken to test the surface roughness at a relatively large area. As presented in Fig. 1d and e, before and after the lubricant infused, there are no obvious roughness changes on the surface of Cu-CAT-1, indicating the nanowires are uniformly arranged on the surface without large micro-scale protuberances.
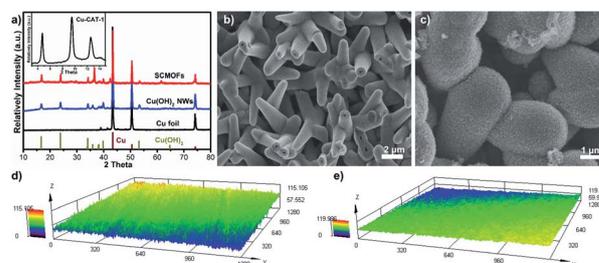

Fig. 1 (a) X-ray diffraction patterns of Cu foil, Cu(OH)₂ NWs and SCMOFs. Scanning electron microscopy images of Cu(OH)₂ NWs (b) and Cu-CAT-1 (c). The confocal laser scanning microscopy images of Cu-CAT-1 (d) and SCMOFs (e).

The wettability of the material surface is important for the passive anti-icing. The liquid nature of SLIPS boosts mobility of water droplets, which greatly lower the specific adhesion strength located in the ice–substrate interface, making it a promising candidate surface for robust ice-phobic application. Through tested using a contact angle meter, the wettability of the samples were studied by static water contact angle (WCA) and water sliding angle (WSA). As shown in Fig. 2, the WCA of SCMOFs is 102° due to the weak interaction between the water and the lubricant. At the same time, the WSA is 2°, indicating the surface possesses a good slippery property. Furthermore, the sliding motion of a water droplet on the slippery surface was also observed visually by the digital pictures as shown in Fig. 2c and d. At the tilting angle of 5°, it takes only 2.3 s for the water droplet (10 μL) to slip away from the SCMOFs surface with a length of 24 mm. Such surface wettability can effectively reduce the droplet anchored and iced on the surface.

The anti-icing performance of SCMOFs was investigated by water crystallization point and freezing delay time. The heterogeneous crystallization of water initiated at the liquid/solid interface, is then followed by the ice growth. Through *in situ* observation the freezing process of water droplet on the surface by optical microscope, the water crystallization point can be obtained when the droplet transparency is changed with the temperature decreasing to a certain point. As shown in Fig. 3a, the crystallization point for the SCNWs is −9.2 °C, whereas the SCMOFs is 2.2 °C lower than SCNWs. The difference may be caused by the roughness between the two samples. The rougher surface of SCMOFs may produce more air pockets between surface and water, hindering their thermal conduction and therefore decreasing the crystallization point. At the same time, the freezing delay time was also recorded to evaluate the anti-icing performance. As exhibited in Fig. 3b–e, under the −20 °C condition, the water droplet begins to freeze at 235 s, and completely frozen at 245 s for SCNWs. In comparison, the time for SCMOFs is delayed to 286 s and 295 s, respectively, better than the freezing delay time of water droplets on the SCNWs. The results of freezing
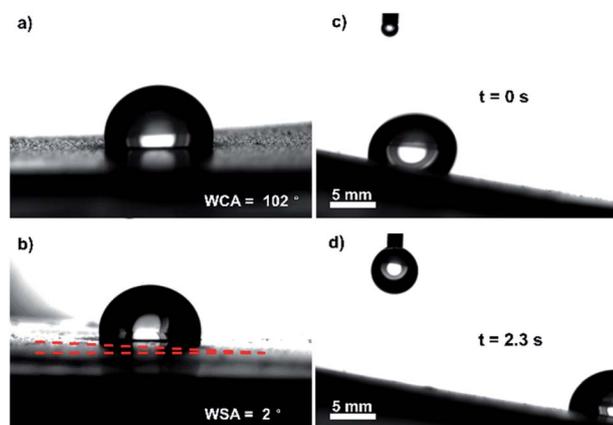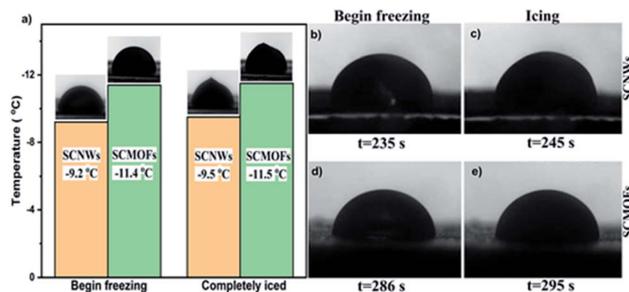

Fig. 3   (a) Freezing point of SCNWs and SCMOFs. Freezing process of water droplets at −20 °C, (b and c) the droplet is on the surface of SCNWs; (d and e) the droplet is on the surface of SCMOFs.

delay time for SCMOFs are well consistent with the water crystallization point, indicating that the SCMOFs possess good anti-icing performance.

The sunlight is a low-cost and infinite energy resource for the outdoor infrastructures especially the working aircraft vehicles in the high altitude. At the same time, the infrared light can penetrate the ice layer to ensure the energy supply. Thus, the sunlight-responsive coating based on the photo-thermal MOFs that could efficiently harvest and convert solar energy to heat is designed for the deicing application. The entire solar spectrum absorption property of the obtained samples were first investigated through the UV-vis-NIR spectroscopy. As shown in Fig. 4a, the SCNWs exhibits a weak light absorption especially at the range of near-infrared light. However, the SCMOFs possesses a superior light absorption almost 100% over the range of solar radiation due to the organic agent in the frameworks. Due to the difference in the light absorption, more light energy was absorbed by the coating to promote the photothermal effect. To evaluate the photothermal performance of different coatings, a sunlamp light was applied as a solar simulator source on the coating surface, the temperature of which was recorded near the irradiated position. Through the time-dependent IR images, the surface temperature of the SCNWs changed little and stabilized at only ~30.3 °C after 20 s of irradiation. In contrast, the temperatures of SCMOFs rose rapidly during irradiation, and reached the plateaus within 20 s as exhibited in Fig. 4b. The high surface temperature will be benefit for the anti-icing/de-icing on the surface of SCMOFs.

The strong light absorption and high heat conversion will be much useful for the anti-icing/de-icing performance. As proved

Fig. 2   (a) The WCA and (b) the WSA of SCMOFs. (c and d) The motion of droplet on the surface of SCMOFs.
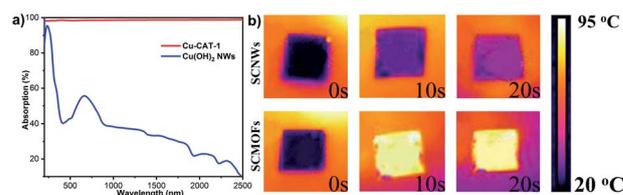

Fig. 4   (a) Light absorption spectra of SCNWs and SCMOFs in the range of solar spectrum (200–2500 nm). (b) Time-dependent IR images of SCNWs and SCMOFs under light illumination.
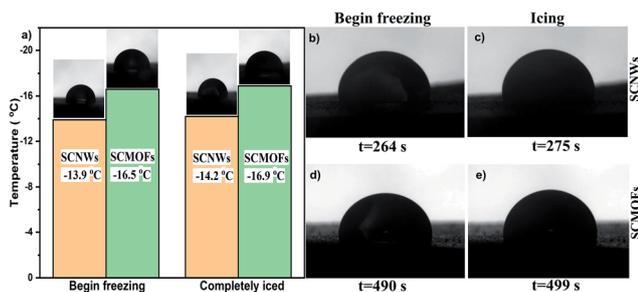
Fig. 5 (a) Freezing point of SCNWs and SCMOFs under the light irradiation. Freezing process of water droplets at −20 °C under the light irradiation, (b and c) the droplet is on the surface of SCNWs; (d and e) the droplet is on the surface of SCMOFs.

in Fig. 5a, the water crystallization point and freezing delay time are investigated to value the light-thermal anti-icing/de-icing performance. Under the light illumination, the water crystallization point of SCMOFs exhibits an obvious decrease to −16.5 °C, contrastively, that of SCNWs shows a weak decrease of temperature in same conditions, indicating the light responsive MOFs can efficiently enhance the anti-icing/de-icing performance. At the same time, the speed of the water crystallization is slowed under the light illumination, as displayed in Fig. 5b and d, the freezing delay time of SCMOFs is prolonged to 490 s, 204 s longer than that without the light illumination. In the same test, the freezing delay time of SCNWs is only 29 s longer due to the weak light absorption and light-thermal conversion of Cu(OH)$_2$ NWs. Furthermore, the melting process of iced droplet on SCMOFs is also investigated. The iced droplet was place on the surface of SCMOFs under the room temperature. As shown in Fig. 6 and Video 1,† after locally irradiated by an 808 nm NIR laser, the iced droplet began to melt from the bottom due to the excellent photo-thermal conversion ability of SCMOFs. At the same time, owing to the good slippery property, the half-melted droplet began to move with a fast speed (20 mm with 15 s). For comparison, without the irradiation, the iced droplet began to melt and move with more times. At the same time, to further simulating the practical application, the samples were placed in the refrigerator for 24 h to ensure the ice formation. Followed, the samples were irradiated. As shown in the Video 2,† the ice on the surface of SCMOFs can be melted
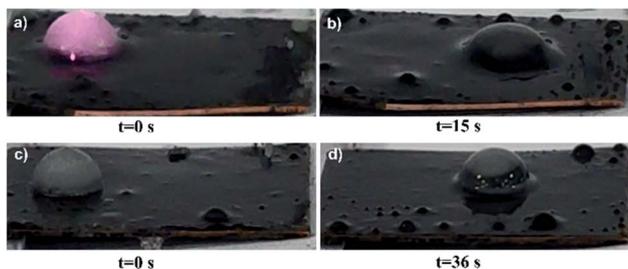
and slipped faster than the ice on the surface of SCNWs. All the results have proven that the light responsive MOFs can enhance the anti-icing/de-icing property under the light illumination, which is highly favorable to be applied in the outdoor infrastructures.

Conclusions

In conclusion, the SCMOFs were successfully fabricated through a simple *in situ* growth method based on the Cu(OH)$_2$ NWs. The obtained SCMOFs possessed good anti-icing/de-icing performance with lowing the water crystallization point and delaying the freezing time. Furthermore, thanks to the strong light absorption and high light-thermal conversion, the SCMOFs showed enhanced anti-icing/de-icing performance with the assist of light illumination. The water crystallization point is low to −16.5 °C and freezing delay time is 204 s longer than that without the light illumination. Meantime, due to the good slippery surface, the half-melted droplet is began to move, which is favorable for the ice removed. This work will provide a new insight into construction of efficient anti-icing materials and make them more suitable for the outdoor infrastructures.

Author contributions

All author contributions equally in this work.

Conflicts of interest

There are no conflicts to declare.

Acknowledgements

Notes and references

1 B. Yu, Z. Sun, Y. Liu, Z. Zhang, Y. Wu and F. Zhou, *ACS Appl. Mater. Interfaces*, 2021, **13**, 37609–37616.
2 S. Zhang, J. Huang, Y. Cheng, H. Yang, Z. Chen and Y. Lai, *Small*, 2017, **13**, 1701867.
3 C. W. Lo, V. Sahoo and M. C. Lu, *ACS Nano*, 2017, **11**, 2665–2674.
4 Z. Huang, S. Kaur, M. Ahmed and R. Prasher, *ACS Appl. Mater. Interfaces*, 2020, **12**, 45525–45532.
5 Y. Yu, B. Jin, M. I. Jamil, D. Cheng, Q. Zhang, X. Zhan and F. Chen, *ACS Appl. Mater. Interfaces*, 2019, **11**, 12838–12845.
6 S. Heydarian, R. Jafari and G. Momen, *Prog. Org. Coat.*, 2021, **151**, 106096.
7 K. Maghsoudi, E. Vazirinasab, G. Momen and R. Jafari, *J. Mater. Process. Technol.*, 2021, **288**, 116883.

Fig. 6 Photographs of frozen droplet melted and slipped on the surface of SCMOFs, (a and b) the droplet is under irradiation; (c and d) the droplet is under no irradiation.

8 J. Lv, Y. Song, L. Jiang and J. Wang, *ACS Nano*, 2014, **8**, 3152–3169.

9 Y. Z. Shen, X. H. Wu, J. Tao, C. L. Zhu, Y. K. Lai and Z. Chen, *Prog. Mater. Sci.*, 2019, **103**, 509–557.

10 S. Zhang, J. Huang, Y. Cheng, H. Yang, Z. Chen and Y. Lai, *Small*, 2017, **13**, 1701867.

11 H. K. Zheng, S. N. Chang and Y. Y. Zhao, *Prog. Chem.*, 2017, **29**, 102–118.

12 X. Yao, B. G. Falzon, S. C. Hawkins and S. Tsantzalis, *Carbon*, 2018, **129**, 486–494.

13 F. Zangrossi, F. Xu, N. Warrior, P. Karapappas and X. H. Hou, *J. Compos. Mater.*, 2020, **54**, 3457–3469.

14 Z. Zhao, H. Chen, X. Liu, Z. Wang, Y. Zhu and Y. Zhou, *Surf. Coat. Technol.*, 2020, **404**, 126489.

15 S. S. Latthe, R. S. Sutar, A. K. Bhosale, S. Nagappan, C.-S. Ha, K. K. Sadasivuni, S. Liu and R. Xing, *Prog. Org. Coat.*, 2019, **137**, 105373.

16 S. Zhang, J. Huang, Y. Cheng, H. Yang, Z. Chen and Y. Lai, *Small*, 2017, **13**, 1701867.

17 S. Farhadi, M. Farzaneh and S. A. Kulinich, *Appl. Surf. Sci.*, 2011, **257**, 6264–6269.

18 K. K. Varanasi, T. Deng, J. D. Smith, M. Hsu and N. Bhate, *Appl. Phys. Lett.*, 2010, **97**, 234102.

19 L. Wang, Q. Gong, S. Zhan, L. Jiang and Y. Zheng, *Adv. Mater.*, 2016, **28**, 7729–7735.

20 Y. Li, T. Hu, B. Li, J. Wei and J. Zhang, *Adv. Mater. Interfaces*, 2019, **6**, 1901255.

21 H. F. Bohn and W. Federle, *Proc. Natl. Acad. Sci. U. S. A.*, 2004, **101**, 14138.

22 W. Cui and T. Pakkanen, *Appl. Surf. Sci.*, 2020, **504**, 144061.

23 K. Golovin, S. Kobaku, D. Lee, E. DiLoreto, J. Mabry and A. Tuteja, *Sci. Adv.*, 2016, **2**, e1501496.

24 R. Yan, T. Ma, M. Cheng, X. Tao, Z. Yang, F. Ran, S. Li, B. Yin, C. Cheng and W. Yang, *Adv. Mater.*, 2021, **33**, 2008784.

25 X. Zhao, Y. Wang, D.-S. Li, X. Bu and P. Feng, *Adv. Mater.*, 2018, **30**, 1705189.

26 Q. Ma, P. Yin, M. Zhao, Z. Luo, Y. Huang, Q. He, Y. Yu, Z. Liu, Z. Hu, B. Chen and H. Zhang, *Adv. Mater.*, 2019, **31**, 1808249.

27 M. Hmadeh, Z. Lu, Z. Liu, F. Gándara, H. Furukawa, S. Wan, V. Augustyn, R. Chang, L. Liao, F. Zhou, E. Perre, V. Ozolins, K. Suenaga, X. Duan, B. Dunn, Y. Yamamto, O. Terasaki and O. M. Yaghi, *Chem. Mater.*, 2012, **24**, 3511.